

SPIFEX Contamination Studies

Engineering Directorate

**Manufacturing, Materials, and Process Technology
Division**

Steven L. Koontz, Johnson Space Center

Orlando Melendez, Kennedy Space Center

Mike Zolensky, Johnson Space Center

Carlos Soares, McDonnell Douglas Aerospace

May 1996

**National Aeronautics and
Space Administration**

**Lyndon B. Johnson Space Center
Houston, Texas**

Contents

	Page
Introduction and Background	1
SPIFEX Hypergolic Engine Exhaust Plume Exposure	1
SPIFEX Payload Preflight and Postflight Photographic Survey	5
Witness Coupon Surface Analysis Methods and Results	6
SEM-EDS Imaging Studies: Engine Plume Particle Impact Damage	6
XPS Surface Analysis	7
Summary and Conclusions	9
Appendixes	
I SPIFEX Contamination Witness Coupons	17
2 SPIFEX Coupons and Ground Control Sample	37

Tables

	Page
I SPIFEX External Contamination Analysis	2
2 Solar Absorptance and Infrared Emittance of the SiO _x -Coated Kapton Surface Film on the SPIFEX Flight Load Measurement Plate and the Corresponding Ground Control Plate	6

Figures

1a NASA Photo S94-36825:	Preflight	11
1b NASA Photo S94-44166:	Postflight	11
2a NASA Photo S94-36824:	Preflight	12
2b NASA Photo S94-44167:	Postflight	12
3a NASA Photo S94-36829:	Preflight	13
3b NASA Photo S94-4417 1:	Postflight	13
4a NASA Photo S94-36807:	Preflight	14
4b NASA Photo S94-44161:	Postflight	14
5 NASA Photo S83-29867:	Damage to Orbiter body flap tiles	15
1-1 Control Sample 1, 7.44X		22
1-2 Control Sample 1, 103X		22
1-3 Control Sample 1, 493X		23
1-4 SPIFEX Witness Coupon 1, 10X		24
1-5 SPIFEX Witness Coupon 1, 101X		24
1-6 SPEFEX Witness Coupon 1, 508X		25
1-7 SPIFEX Witness Coupon 1, 508X		25
1-8 SPIFEX Witness Coupon 1, 1010X		26

1-9 SPIFEX Witness Coupon 1, 1000X	26
1-10 Kapton from Witness Coupon 1, 75 \times , 1020X	27
1-11 Kapton from Witness Coupon 1, 75 \times , 2070X	27
1-12 Witness Coupon 1, Aluminum Area 75 \times , 1150X	28
1-13 Witness Coupon 1, Aluminum Area 75 \times , 2070X	28
1-14 Kapton from Witness Coupon 1, 521X	29
1-15 Kapton from Witness Coupon 1, 1480X	29
1-16 Witness Coupon 2, 10.5X	30
1-17 Witness Coupon 2, 99.4X	30
1-18 Witness Coupon 2, 497X	31
1-19 Kapton from Witness Coupon 2, 101 X	32
1-20 Kapton from Witness Coupon 2, 508X	32
1-21 Witness Coupon 3, 14.8X	33
1-22 Witness Coupon 3, 105X	33
1-23 Witness Coupon 3, 516X	34
1-24 Kapton from Witness Coupon 3, 103X	35
1-25 Kapton from Witness Coupon 3, 508X	35
2-1 Typical view od SPIFEX flight coupon 1 showing many small craters	40
2-2 Typical round crate; this one contains no detectable impactor residue	40
2-3 Elliptical crater with Cr-containing grains (all measuring less than 0.3 micrometers), interpreted as forming from an oblique impact by a CR- containing impactor	41
2-4 The crater in the center has a small grain(approximately 1 micrometer) of Fe, interpreted as being residue from an FE-bearing impactor	41

SPIFEX Contamination Studies

Introduction and Background

The Shuttle Plume Impingement Flight Experiment (SPIFEX) was completed during STS-64. SPIFEX was designed to produce accurate measurements of rocket engine exhaust plume impingement (1) forces, (2) heating effects, and (3) static and dynamic pressures caused by the operation of the Space Shuttle Primary Reaction Control System (PRCS) and Vernier Reaction Control System (VRCS) engines. Data on plume impingement effects is needed to support both the assessment of Space Station - Space Shuttle proximity operations planning and the verification of Space Station performance requirements as a part of the ongoing design review process. A description of the SPIFEX flight experiment as well as the results of the plume force, thermal effects and static/dynamic pressure measurements is available in JSC-27030, "Shuttle Plume Impingement Flight Experiment (SPIFEX) Test Report, Vol. 1 - Test Description and Results," J. R. Hughes, S. M. Fitzgerald, R. A. Machin, M. J. Stubner, A. R. Rocha, K. S. Leahy, W. C. Rochelle, and M. K. White, December 1995.

Contamination of functional surfaces, and other types of surface degradation, resulting from rocket engine exhaust plume impingement are also the subject of Space Station program requirements documents such as SSP-30426 and SSP-30233, and assessing the compliance of the Space Station design with the subject requirements is an important part of the design review process. The SPIFEX flight experiment also produced data on contamination and materials degradation effects. Witness coupons placed on the static/dynamic pressure measurement assembly were analyzed for hypergolic engine residues after the mission by X-ray photoelectron spectroscopy (XPS, in which the elemental composition of a solid is determined to a depth of 50 to 100 angstroms). Surface damage produced by high-speed particles in the rocket engine exhaust plume was analyzed by scanning electron microscopy (SEM) combined with energy dispersive X-ray spectroscopy (EDS, in which the SEM electron beam is used to excite X-ray spectra for elemental analysis). In addition, preflight and postflight photographic surveys were made of the SPIFEX hardware to document any changes in the appearance of the hardware resulting from STS-64 flight operations.

This JSC Report documents the results of the SPIFEX contamination and materials degradation studies.

SPIFEX Hypergolic Engine Exhaust Plume Exposure

The witness coupons were exposed to the same PRCS and VRCS engine firings as the SPIFEX pressure measurement plate. The contamination measurement coupons were placed on the pressure measurement plate within 1 cm of a temperature measurement sensor. Table 1 summarizes the SPIFEX engine firing history including engine identity, engine nozzle to SPIFEX distance (in units of feet and nozzle throat radii; PRCS Re = 3.73 in., VRCS Re = 0.4 1), witness coupon surface temperature, angle of attack for plume gas flow over the witness coupons, and the number of degrees the witness coupons were placed off the engine plume axis.

Two important features of the data presented in table 1 should be noted. First, the surface temperature of the witness coupons was well below 270° K for nearly all the PRCS and vernier firings, and no significant surface heating resulting from engine plume gas impingement could be detected. Second, PRCS and VRCS engine firing duration was 240 milliseconds, a departure from the 80 millisecond pulsed firing duration usually employed in Space Shuttle operations.

Test #	Fire MET	Flt Day	temp1	temp2	Jet	R/Re	Θ	I	Dur. (ms)	Dis. (ft)	Mass Flux (gm/cm**2/sec)	Total Mass Flux (gm/cm**2)
PRCS Firings												
11	1:00:54:35	2	257.1	257.2	F3U	150	35	0	240	60	1.2917E-04	0.000031
12	1:01:10:17	2	263.4	263.7	F3U	190	0	0	240	76	2.5118E-04	0.000060
13		2			F3U	190	0	0	240	76	2.5118E-04	0.000060
14	1:01:21:45	2	266.3	266.8	F3U	190	0	90	240	76	2.5118E-04	0.000000
15	1:01:26:00	2	269.6	269.6	F3U	150	0	0	80	60	4.0301E-04	0.000032
16	1:01:29:20	2	275.7	270.2	F3U	150	0	0	240	60	4.0301E-04	0.000097
17	1:01:38:02	2			F3U	150	0	0	720	60	4.0301E-04	0.000290
18	1:01:44:15	2	278	277.7	F3U	150	0	15	240	60	4.0301E-04	0.000093
19	1:01:48:30	2	274	273.8	F3U	150	0	15	240	60	4.0301E-04	0.000093
20	1:01:51:32	2	271.4	271.1	F3U	150	0	45	240	60	4.0301E-04	0.000068
21	1:01:55:17	2	268.3	268.2	F3U	150	0	90	240	60	4.0301E-04	0.000000
22	1:01:06:05	2	261.4	261.2	F3U	100	0	0	240	40	9.0677E-04	0.000218
23	1:02:09:20	2			F3U	100	0	60	240	40	9.0677E-04	0.000109
24	1:02:13:16	2			F3U	100	0	87	240	40	9.0677E-04	0.000011
25	1:02:26:53	2	259	259.1	F3U	200	35	87	240	80	7.2659E-05	0.000001
26	1:02:30:38	2	261.2	261.5	F3U	200	35	0	240	80	7.2659E-05	0.000017
27	1:02:33:25	2	263.8	264.1	F3U	200	35	0	240	80	7.2659E-05	0.000017
28		2	265.7	265.9	F3U	200	20	0	240	80	1.5854E-04	0.000038
29	1:02:42:32	2	266.3	266.3	F3U	150	35	0	240	60	1.2917E-04	0.000031
30	1:02:47:44	2	265.6	265.5	F3U	150	15	0	240	60	3.3020E-04	0.000079
31	1:02:53:36	2	266	266.1	F3U	150	35	0	240	60	1.2917E-04	0.000031
32	1:02:58:56	2	266.7	266.7	F3U	150	60	0	240	60	1.3399E-05	0.000003
33	1:03:01:40	2	266.7	266.7	F3U	150	60	0	240	60	1.3399E-05	0.000003
34	1:03:05:24	2	266.8	266.8	F3U	150	75	0	240	60	3.1482E-06	0.000001
52	1:19:36:34	3	277.4	277.3	F1F	125	30	0	240	50	2.5472E-04	0.000061
53		3	272.8	272.7	F1F	125	30	0	240	50	2.5472E-04	0.000061
54	1:19:49:06	3	270.2	269.9	F1&2F	125	30	0	240	50	2.5472E-04	0.000061
55	1:19:52:46	3	267.9	267.8	F1F	125	30	90	240	50	2.5472E-04	0.000000
56	1:19:58:00	3	264.5	264.3	F1F	125	30	0	240	50	2.5472E-04	0.000061
57	1:20:01:22	3	262.6	262.5	F1&2F	125	30	0	240	50	2.5472E-04	0.000061
58	1:20:09:51	3	258.4	258.2	F1F	125	0	0	240	50	5.8033E-04	0.000139
59	1:20:13:56	3	256.7	256.7	F1F	125	15	0	240	50	4.7549E-04	0.000114
60	1:20:20:43	3	256.1	265.1	F1F	125	30	0	240	50	2.5472E-04	0.000061
61	1:20:22:23	3	256.5	256.5	F1&2F	125	30	0	240	50	2.5472E-04	0.000061
62	1:20:25:47	3	259.2	259.7	F1F	125	30	90	240	50	2.5472E-04	0.000000

Test #	Fire MET	Flt Day	temp1	temp 2	Jet	R/Re	Θ	T	Dur. (ms)	Dur. Dis. (ft)	Mass Flux (gm/cm**2/sec)	Total Mass Flux (gm/cm**2)
63	1:20:31:53	3	262.5	262.5	FIF	125	30	0	240	50	2.5472E-04	0.000061
64	1:20:36:23	3	264.3	264.5	FIF	125	45	0	240	50	8.2108E-05	0.000020
65	1:20:53:27	3	268.8	268.8	F1&2F	125	15	0	240	50	5.8038E-04	0.000139
66	1:20:58:44	3	269.7	269.7	F1&2F	125	15	0	240	50	4.7549E-04	0.000114
67	1:21:04:09	3	269.7	269.7	F1&2F	100	0	0	240	40	9.0677E-04	0.000218
68	1:21:08:27	3	269.2	269.2	F1&2F	80	0	0	240	32	1.4168E-03	0.000340
69		3			F1&2F	80	0	0	240	32	1.4168E-03	0.000340
70		3	266	265.9	F1&2F	100	30	0	240	40	3.9800E-04	0.000096
71		3	264.3	264.2	F1&2F	125	30	0	240	50	2.5472E-04	0.000061
72	1:21:25:00	3	261.9	261.8	F1&2F	125	60	0	240	50	1.9294E-05	0.000005
73	1:21:29:50	3	259.1	259.0	F1&2F	150	60	87	240	60	1.3399E-05	0.000000
74	1:21:34:23	3	256.1	256.0	F1&2F	150	60	87	240	60	1.3399E-05	0.000000
75	1:21:41:14	3	252.9	252.9	F1&2F	150	60	0	240	60	1.3399E-05	0.000000
76	1:21:47:21	3	253.4	253.5	F1&2F	150	90	87	240	60	7.3970E-07	0.000000
77	1:21:57:31	3	255.6	255.8	F1&2F	150	90	0	240	60	7.3970E-07	0.000000
83	2:15:48:44	4	262.4	262.5	L2L	100	0	42	240	40	9.0677E-04	0.000162
84	2:15:55:39	9			L2L	100	0	42	240	40	9.0677E-04	0.000162
85		9			L2L	100	30	0	240	40	3.9800E-04	0.000096
86		9			L2L	100	60	0	240	40	3.0147E-05	0.000007
101	2:15:51:21	4	263.4	263.7	L2L	100	0	42	720	40	9.0677E-04	0.000485
102	2:15:53:46	4	265.3	265.7	L2L	100	0	72	240	40	9.0677E-04	0.000067
103					L2L	100	0	102	240	40	9.0677E-04	0.000045
104					L2L	100	0	122	240	40	9.0677E-04	0.000115
105		9	259.8	259.7	L3L	100	0	0	240	40	9.0677E-04	0.000218
106		9	254.8	254.7	F3U	150	0	15	240	60	4.0301E-04	0.000093
113		9	251.9	251.8	F3U	125	45	0	240	50	8.2108E-05	0.000020
114		9	250.9	250.8	FIF	127	79.5	?	240	51	3.0810E-06	
115		9	250.1	249.9	F1&2F	127	79.5	-4.5	240	51	3.0810E-06	0.000001
118		9	250.2	250.2	FIF	124	52.6	?	240	50	3.7928E-05	
119		9	250.2	250.1	F1&2F	125	52.9	0	240	50	3.7928E-05	0.000009
122		9	249.7	249.7	FIF	124	37.5	?	240	50	1.4966E-04	
123		9	249.7	249.7	F1&2F	125	37.9	0	240	50	1.4966E-04	0.000036
124		9	250.2	250.3	FIF	124	37	?	240	49	1.6131E-04	
125		9	250.5	250.4	F1&2F	125	37.9	0	240	50	1.4966E-04	0.000036
126		9	252	252.0	FIF	123	36.8	?	240	49	1.6131E-04	
127		9	252.2	252.2	F1&2F	125	37.9	0	240	50	1.4966E-04	0.000036
107		9	252	252.1	F3U	125	15	0	240	50	4.7549E-04	0.000114

SPIFEX Payload Preflight and Postflight Photographic Survey

Visual inspection and photographic documentation of the SPIFEX flight hardware both before and after the SPIFEX flight showed no visible evidence of contamination or damage resulting from engine plume impingement.

Figures 1a and 1b show photographs of a SPIFEX surface immediately adjacent to the payload plume sensor package both before (1a) and after (1b) the spaceflight experiment. The surface shown in the photograph is aluminum painted with A-276, a polyurethanebased white space paint. There is no evidence of damage from hypergolic engine plume impingement during SPIFEX either in the photo or by visual inspection.

The preflight and postflight photos of the pressure measurement plate and the contamination measurement witness coupons, visible as five metallic disks in a trapezoidal Kapton™ tape coupon holder, are shown in figures 2a and 2b, respectively. Once again, little change in appearance is evident in the photographs, beyond the small changes attributable to changes in lighting conditions. Postflight visual inspection showed no change in appearance compared to the preflight appearance.

Figures 3 and 4 also compare the preflight and postflight appearance of SPIFEX hardware components which were exposed to hypergolic engine plume impingement. In all cases, visual inspection revealed little or no difference in the appearance of the various SPIFEX components resulting from the spaceflight experiment.

The video camera assembly shown in figure 3 reveals no evidence of degradation resulting from SPIFEX operations. The assembly was positioned within 20 cm of the witness coupons and received essentially the same engine plume impingement history. The nearly pristine appearance of this delicate instrument assembly supports the general conclusion of this report that the limited hypergolic engine plume impingement characteristic of proximity operations produces no gross materials or systems degradation. The quartz window held by the white circular Teflon™ ring visible in the photos was sent to NPO Energia for independent analysis of plume impingement effects.

The SiO_x-coated Kapton surface of the load measurement plate (figure 4) did show some slight variation in appearance, though not the darkening apparent in the figures (variation in photo lighting conditions). The appearance of some regions of the SiO_x-coated Kapton did change as a result of the spaceflight and is attributed to changes in the properties of the adhesive bonding surface. Thermo-optical property measurements on both the ground control and flight plates showed no significant difference between the two. Measurements of the solar absorptance, α , and the infrared emittance, ϵ , measured at five randomly selected points on each plate gave the results shown in table 2.

Table 2 Solar Absorptance and Infrared Emittance of the SiO_x-Coated Kapton Surface Film on the SPIFEX Flight Load Measurement Plate and the Corresponding Ground Control Plate

Measurement	α,SPIFEX	α,Control	ε,SPIFEX	ε,Control
Result	plate	plate	plate	plate
average	0.673	0.690	0.860	0.864
std. dev.	0.012	0.014	0.009	0.002

It is significant that the Kapton tape trapezoid holding down the witness coupons did not develop a diffuse surface, during the mission, as a result of atomic oxygen exposure. The absence of direct evidence of atomic oxygen attack is not surprising because SPIFEX operations were conducted at a relatively high altitude during solar minimum so that a total oxygen atom fluence of less than 10^{19} atoms/cm² was anticipated and that fluence is not sufficient to produce a diffuse surface on a glossy Kapton tape.

Witness Coupon Surface Analysis Methods and Results

The aluminum foil witness coupons and the Kapton tape used to affix the coupons to the pressure measurement plate were characterized by XPS (SEM with EDS). Flight coupons and tape were compared to control samples prepared at the same time and with identical procedures and stored under controlled conditions in the JSC materials laboratory in clean fluorocarbon sample containers. The witness coupons and tape holder were removed from the SPIFEX payload and inspected, at JSC, after the postflight photo survey and inspection. The witness coupons and associated tape were then sent to KSC for analysis by XPS and SEM. Control and flight samples were shipped by Federal Express™ using clean fluorocarbon containers.

SEM-EDS Imaging Studies: Engine Plume Particle Impact Damage

SEM photomicrographs of the aluminum foil witness coupons, the Kapton tape holding the witness coupons to the pressure plate, and the corresponding ground controls are shown in Appendix 1, figures 1-1 - 1-25 and in Appendix 2, figures 2-1 - 2-4. Particle impact craters are visible on all witness coupon photomicrographs with magnifications greater than or equal to about 100X. The particle craters on the Kapton tape specimens are both more numerous and of a different morphology than those in the aluminum foil samples. The craters in both aluminum and Kapton result from the direct impingement of unburned fuel and oxidizer droplets produced by the Space Shuttle hypergolic engines that were fired at the SPIFEX payload during the flight experiment.

The presence of short-lived monomethylhydrazine (MMH) and oxidizer (N_2O_4) droplets in hypergolic engine exhaust plumes is a well known phenomena. The droplets evaporate rapidly in the hot exhaust plume gases; however, the same hot gases accelerate the droplets to exhaust plume speeds rapidly so that the particles can strike nearby surfaces before evaporating completely. Pulsed operation of hypergolic engines is expected to produce more droplets than prolonged burns. Figure 5 shows the damage to the Space Shuttle Orbiter body flap tiles produced by several thousand firings of the VRCS engine which is directed at the body flap; 12 mil (0.3 mm) of the black reaction cured glass coating has been completely removed. In addition, Trinks and Hoffman ("Experimental Investigation of Bipropellant Exhaust Plume Flowfield, Heating and Contamination, and Comparison With the CONTAM Computer Model Predictions," AIAA-83-1447, 18th Thermophysics Conference, June 1-3, 1983) have made direct measurements of the droplet flux produced by a small hypergolic thruster and verified the predictions of the CONTAM hypergolic engine simulation code.

Application of an early version of the CONTAM code to Space Shuttle PRCs and VRCS engines suggested that the fraction of unburned propellant in the form of both droplets and vapor could vary considerably with the size of the engine with larger engines producing a much smaller unburned propellant fraction (R. J. Hoffman, A. W. Kawasaki; "STS RCS and VCS Plume Flowfields," AFRPL TR-85-046, July 1985).

It should be noted that direct release of MMH or N_2O_4 into a space-like vacuum results in the formation of supercooled liquid (MMH) or ice particles (N_2O_4) as a result of adiabatic flash evaporation of the liquid on introduction into the vacuum environment (E. L. Miller, S. L. Koontz; "Characteristics of Liquid Hydrazine, Monomethylhydrazine, Ammonia, and Dinitrogen Tetroxide Sprayed into a Space-Like Vacuum," NASA WSTF TR-355-002, July 2, 1986).

The craters on the Kapton appear to be the result of chemically reactive liquid droplets, probably MMH, impinging at moderate velocity. MMH rapidly dissolves Kapton and other polyimides even at relatively low temperatures. The smaller craters in the aluminum witness coupons were probably formed by impact of solid oxidizer ice particles.

The Kapton tape sample had $1.3 \pm 0.3 \times 10^6$ impacts per square cm while the aluminum witness coupons had $4.4 \pm 0.9 \times 10^5$ impacts per square cm as determined by counting the craters in the 500X SEM photos. No impact features of any kind were found in the ground control samples.

The SEM EDS results reported in Appendix 2 showed that only about 5 percent of the craters had any identifiable impactor residue (only the aluminum witness coupons were analyzed). In most cases, the impactor residue was Fe, though in two cases Cr was detected. The oxidation state of the metals was not determined. Iron and chromium nitrates are the principle corrosion product produced by N_2O_4 in contact with stainless steel and have been implicated in several in-flight failures (e.g., STS-63) of the PRCS-engine oxidizer flow-control valve.

XPS Surface Analysis

Evaluation of the amount of persistent surface contamination produced by Space Shuttle PRCS engines was the main objective of the SPIFEX witness coupon experiment. Persistent surface contamination produced by the PRCS and VRCS engine firings at the SPIFEX payload was determined using XPS to produce quantitative measurements of the nitrogen content in the surface of the aluminum witness coupons. XPS produces data describing the elemental composition, in atom percent, of the 50 angstrom layer nearest the sample surface (as described in the following paragraphs). The XPS analysis results are given in Appendix 1 and the data reduction is presented below.

Nitrogen was selected as the element marking hypergolic engine plume contamination because

Ground-based laboratory measurements have always identified MMH nitrate as the most important condensable combustion by-product (F. G. Etheridge, R. A. Boudreaux; "Attitude Control Rocket Exhaust Plume Effects on Spacecraft Functional Surfaces," J. Spacecraft, 7(1), pp 45-48, January 1970).

Thermodynamic calculations and CONTAM simulations both suggest that nitrate should be expected to form transient MMH nitrate deposits (C.K. Liu, A.P.M. Glassford; "Contamination Effects of MMH/ N_2O_4 Rocket Plume Product Deposit, J. Spacecraft, 18(4), pp 306-311, July-August 1981).

The data of Trinks and Hoffman (previously cited) showed that under some circumstances, the hypergolic engine plume deposits may become persistent as a result of exposure to oxygen plasma discharge conditions (a crude simulation of low-Earth orbit).

The ground control samples (see Appendix 1) showed no evidence of nitrogen in the XPS spectrum while the flight coupons showed an average of 1.917 ± 0.266 atom percent nitrogen. The quantity of interest in contamination assessments and contamination control is the number of micrograms per square centimeter. The data analysis problem becomes one of converting atom percent in the XPS surface sampling volume to micrograms per square centimeter of MMH nitrate on the witness coupons. We will report any nitrogen detected as nitrate. Estimating the XPS sampling volume and the density of the material in that sampling volume are the key steps in data analysis.

The XPS detects the X-ray photoelectrons emitted from a solid being bombarded with X-rays. The XPS spectrum consists of a plot of the number of electrons in each kinetic energy interval plotted against the electron kinetic energy. The energy of the X-rays is very well defined, so that chemical elements, and often their oxidation states, can be determined by simply measuring the kinetic energy spectrum of the X-ray photoelectrons, which will be the difference between the energy of the X-ray and the electron binding energy of a particular electron shell in the parent atom. The extreme surface sensitivity of the XPS method results from the very short collision length of X-ray photoelectrons in solids; that is, the photoelectron can't escape the solid and retain kinetic energy information unless that photoelectron is created within a very few collision lengths of the surface.

Measurements of electron escape depths in the element Si indicate that 15 angstroms is the best and most recent value (C.J. Powell, M.P. Seah; "Precision, Accuracy and Uncertainty in Quantitative Surface Analysis by Auger-electron Spectroscopy and X-ray Photoelectron Spectroscopy," J. Vac. Sci. Technol., A8 (2), pp 735-768, March-April 1990). No escape depth measurements have been reported in the open literature for Al or Al_2O_3 . The escape depth used for analysis of the SPEFEX contamination witness coupon data is estimated as the escape depth of Si corrected by the Si/ Al_2O_3 density ratio because the photoelectron collision length in a solid is proportional to the density of the solid.

The number of photoelectrons escaping from some distance, x , below the surface is a function of both the collision length and x . Thus, with an escape length of 15 angstroms, 2.3 grams per cubic centimeter for the density of Si, and 3.5×0.858 grams per cubic centimeter for the density of gamma alumina (corrected for the actual elemental composition measured by XPS as described in the next paragraph) we have,

$$T = \int_0^{100} \exp\left(-\frac{x \frac{2.3}{3.50.858}}{15}\right) dx \quad T_s = \int_0^{50} \exp\left(-\frac{x \frac{2.3}{3.50.858}}{15}\right) dx$$

$$\frac{T_s}{T} = 0.928$$

where T is the total signal from all depths, x, less than or equal to 100 angstroms and Ts is the total signal escaping from all depths less than or equal to 50 angstroms. Clearly, a sampling depth of 50 angstroms will account for 93 percent of the photoelectrons escaping from the sample, so 50 angstroms will be used as the sampling depth for the analysis reported here.

The actual elemental composition of the surface film as measured by XPS is different from that for pure, low-density, $-\text{Al}_2\text{O}_3$. The average surface film elemental composition of the three SPIFEX corresponds to a formula weight of 17.483 amu compared to 20.4 amu for pure $-\text{Al}_2\text{O}_3$, so that the surface film sampled by XPS has a density 0.858 times that of the pure aluminum oxide (3.5 g/cc). The total mass (per square cm) of the surface film sampled by XPS is then,

$$(50 \times 10^{-8}) (3.5) (0.86) = 1.505 \times 10^{-6} \text{ micrograms/cm}^2$$

The total mass of nitrogen in the film is calculated from the atomic weight of nitrogen and the average surface atom percent nitrogen for the three samples or,

$$\frac{14 \frac{1.917}{100}}{17.483} = 0.0015 \text{ percent nitrogen by weight.}$$

Given that (1) MMH nitrate is 38.5 percent nitrogen by weight and (2) the total plume gas flow to the witness coupons is 0.005212 grams per square centimeter, the average value of the hypergolic engine exhaust gas sticking fraction (the mass fraction of the plume gases sticking permanently to the SPIFEX witness coupon surface calculated as MMH nitrate) can be calculated as,

$$(1.5 \times 10^{-6}) (0.015) \left(\frac{1}{0.385}\right) \left(\frac{100}{0.005212}\right) = 0.001 \text{ percent mass}$$

Summary and Conclusions

The combined PRCS and VRCS hypergolic engine exhaust plume flow to the SPIFEX witness coupons left 0.001 percent of the net plume mass flow in the form of MMH nitrate or some similar compound. Particle impact craters were observed on both the aluminum witness coupons and the Kapton sample holder tape, with a much higher impact crater count on the tape than on the aluminum. The particle impact craters are probably the result of unburned fuel or oxidizer droplets produced by the engines during operation. The CONTAM hypergolic engine simulation software predicts that larger numbers of droplets come from VRCS than from PRCS. The SPIFEX data provides no way to directly attribute the particles to a specific engine set.

Because the temperature of the SPIFEX witness coupons was measured to be on the order of -30 centigrade, the contamination data produced here corresponds to a "worst case" condition for many Space Station functional surfaces and a nominal case for the ATCS radiators. The Space Station Program can reasonably reduce the hypergolic plume gas sticking fraction from 0.02 to 0.001 percent of the plume gas fluence to any functional surface in future contamination and materials degradation assessments.

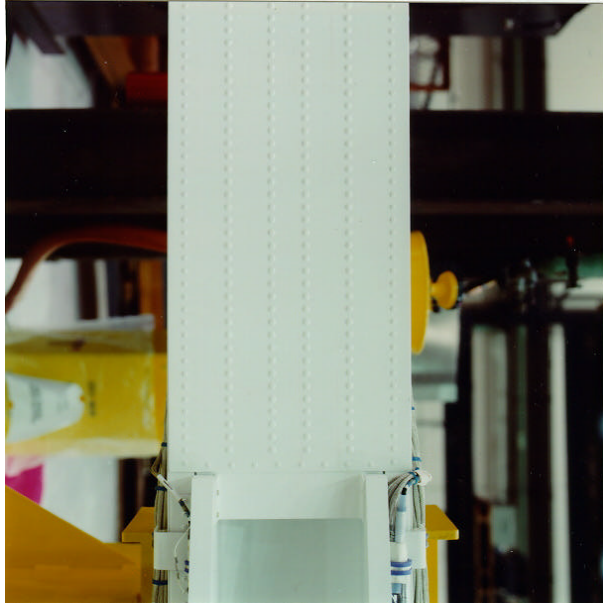


Figure 1a. NASA Photo S94-36825: Preflight

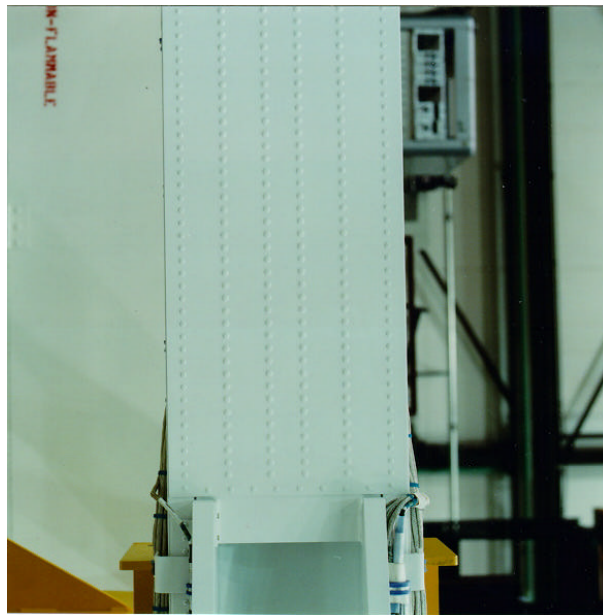


Figure 1b. NASA Photo S94-44166: Postflight

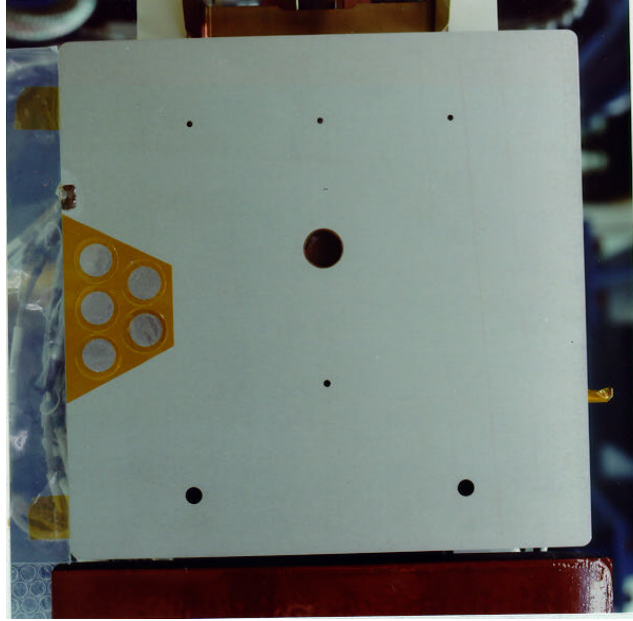


Figure 2a. NASA Photo S94-36824: Preflight

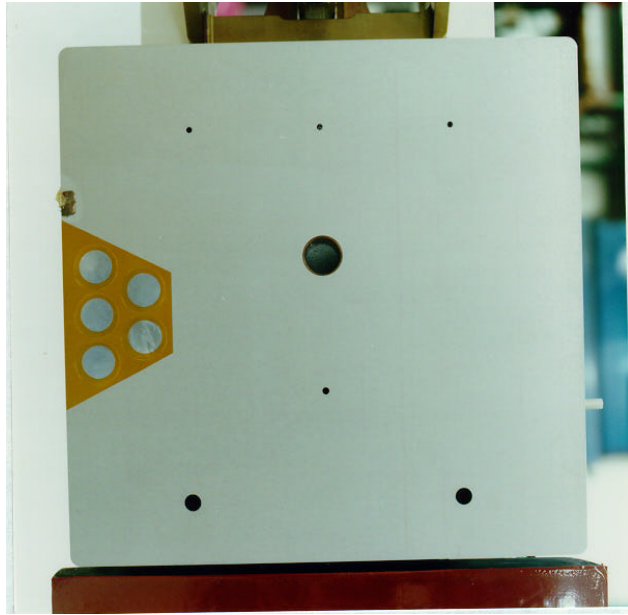


Figure 2b. NASA Photo S94-44167: Postflight

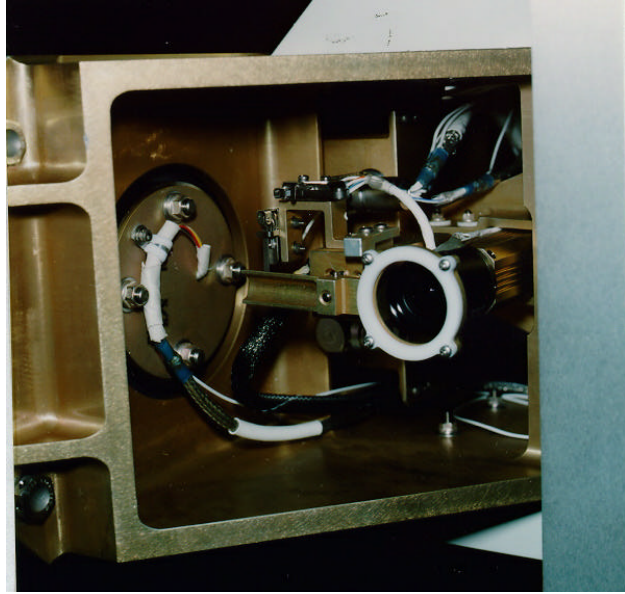


Figure 3a. NASA Photo S94-36829: Preflight

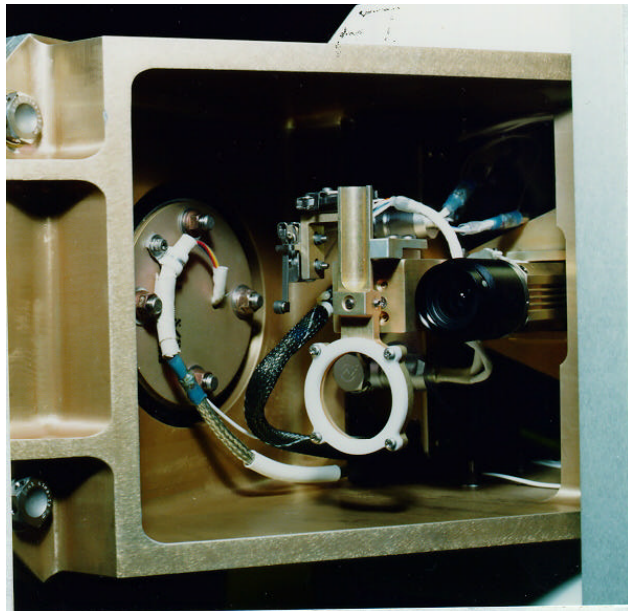


Figure 3b. NASA Photo S94-44171: Postflight



Figure 4a. NASA Photo S94 -36807: Preflight



Figure 4b. NASA Photo S94-44161: Postflight

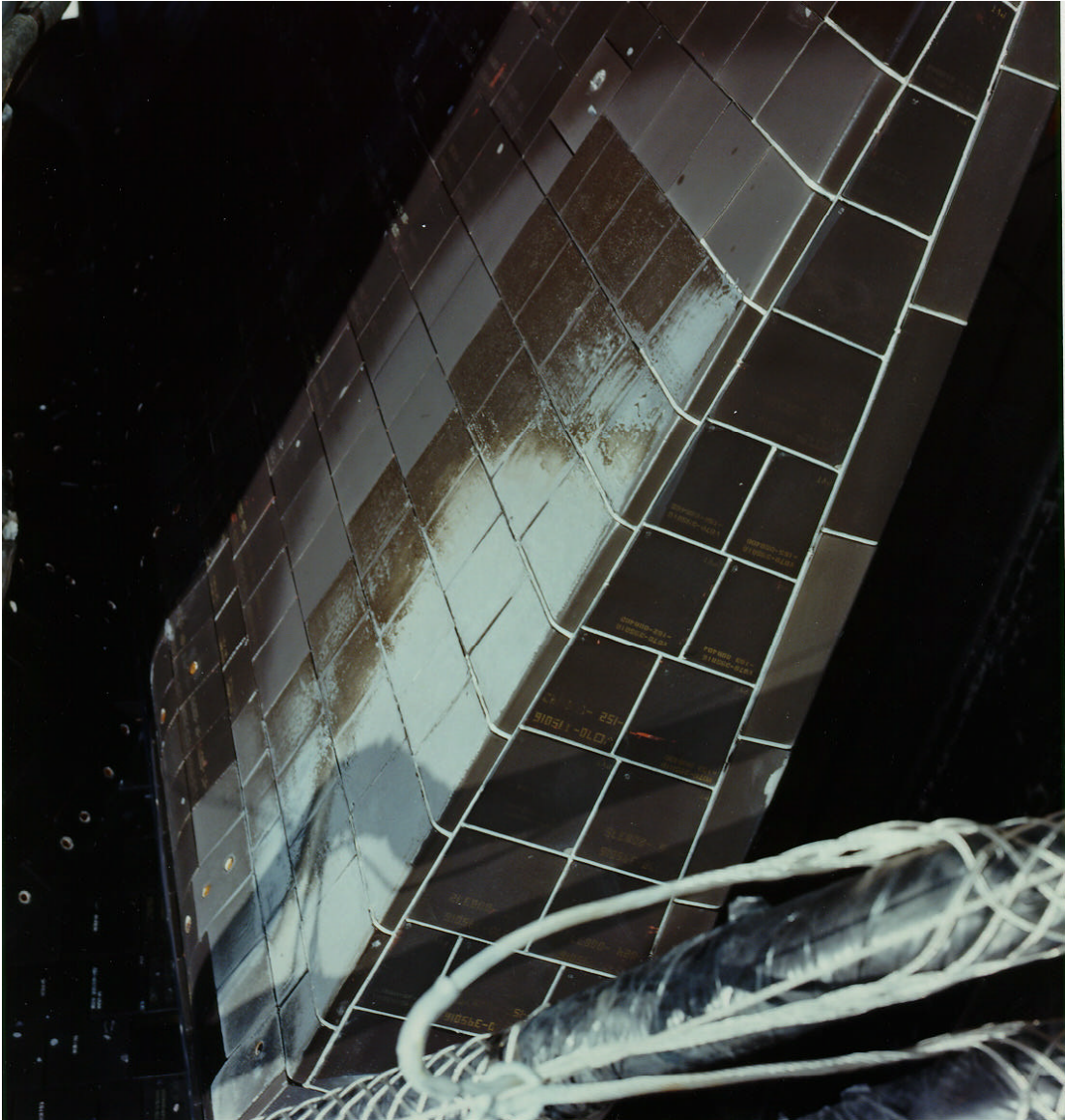


Figure 5. NASA Photo S83-29867: Damage to Orbiter body flap tiles

MATERIALS AND CHEMICAL ANALYSIS BRANCH
DM-MSL-1C, ROOM 1274, O&C BUILDING
NASA/KSC

December 2, 1994

SUBJECT: Shuttle Plume Impingement Flight Experiment

(SPIFEX) Contamination Witness Coupons

LABORATORY REQUEST NO: MCB 0810-94

1.0 FORWARD:

1.1 REQUESTER: Steven L. Koontz/NASA JSC/EM2-94-113

1.2 REQUESTER'S SAMPLE DESCRIPTION: The SPIFEX (STS-64) exposed a sensor array to Space Shuttle Primary Reaction Control System (PRCS) engine plume impingement events. The primary objective of SPIFEX is measurement of engine plume gas dynamic loads to support Space Shuttle-Space Station proximity operations. Measurements of surface contamination produced by PRCS engine plumes are an important secondary objective of SPIFEX. Three SPIFEX witness coupons and two unflown control samples were submitted for analysis. The Kapton tape used to attach the witness coupons to the SPIFEX payload is still attached to the samples.

1.3 REQUESTED: Surface analysis using X-ray photoelectron Spectroscopy (XPS) and scanning electron spectroscopy (SEM).

2.0 CHEMICAL ANALYSIS AND RESULTS:

2.1 The samples were analyzed using a Kratos XSAM 800 XPS spectrometer. The instrument conditions were Mg X-rays @ 15 mA and 12 kV. The pressure inside the chamber during the analysis was less than 5×10^{-9} torr.

2.2 The XPS results showed aluminum, oxygen and carbon for both control samples.

2.3 All three SPIFEX witness coupon showed aluminum, oxygen, carbon. They also contained silicon, nitrogen and traces of fluorine not observed on the control coupons.

2.4 The XPS results are shown in the following table:

Elements Concentration
(atomic %)

Sample	C	O	Al	Si	N	F
control 1	32.49	43.90	22.94	-	-	.66
control 2	34.02	43.63	22.35	-	-	-
coupon 1	19.35	51.49	19.24	5.74	2.28	1.90
Kapton 1	41.28	41.91	-	10.80	6.01	-
coupon 2	18.99	51.68	19.93	5.26	1.65	2.49
Kapton 2	48.54	38.30	-	7.45	5.70	-
coupon 3	23.15	49.72	19.59	4.19	1.82	1.53

2.5 The binding energy of the peaks in the XPS spectrum were assigned relative to the binding energy of carbon 1s at 284.6 eV. The binding energy of the silicon peak was 101.8 eV for the witness coupon 1, and 102.3 eV for the witness coupons 2 and 3. The binding energy of the silicon peak corresponds to that of the silicones (silanes) group. The observed silicon binding energy for the Kapton samples attached to coupons 1 and 2 was 103 eV which corresponds to silica.

2.6 The observed binding energy for nitrogen was 399.3 eV for the witness coupon 1 and 399.7 eV for witness coupons 2 and 3. These binding energy correspond to a high oxidation state possibly a nitrogen salt. The binding energy for elemental nitrogen is 398.1 eV.

2.7 One control sample and the three witness coupons were examined using scanning electron microscope (SEM). Figures 1-22 show the surfaces of the aluminum control sample and the aluminum and Kapton for the three witness coupons. The control sample has a fairly smooth surface. The aluminum and Kapton surfaces have impact marks. The Kapton surfaces have crater-like "frozen splash" marks. The aluminum surfaces show shallow craters or dents. The craters and dents on both the Kapton and the aluminum surfaces appear to have been caused by drops of liquid impacting the surfaces at high velocity. EDS analyses within the

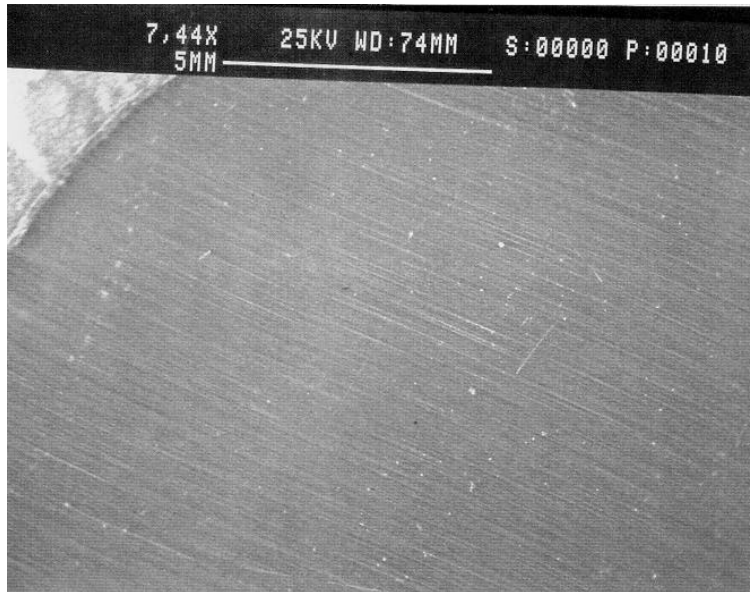


Figure 1-1. Control Sample 1, 7.44X

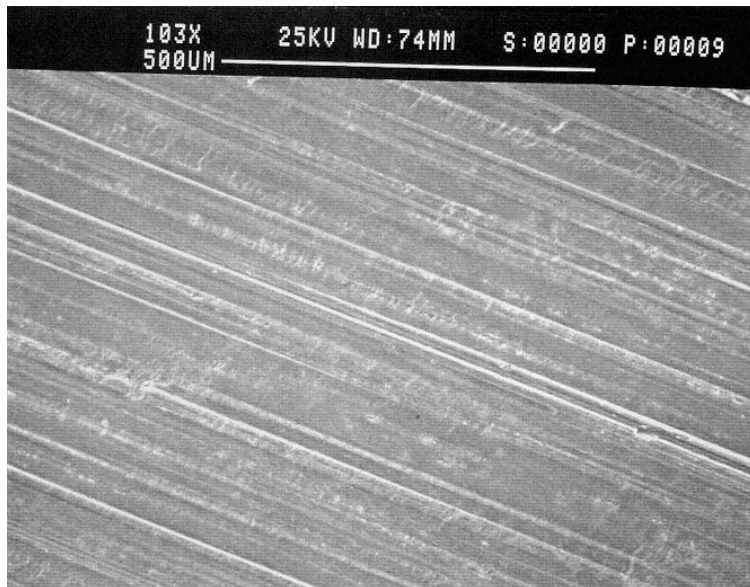


Figure 1-2. Control Sample 1, 103X



Figure 1-3. Control Sample 1, 493X

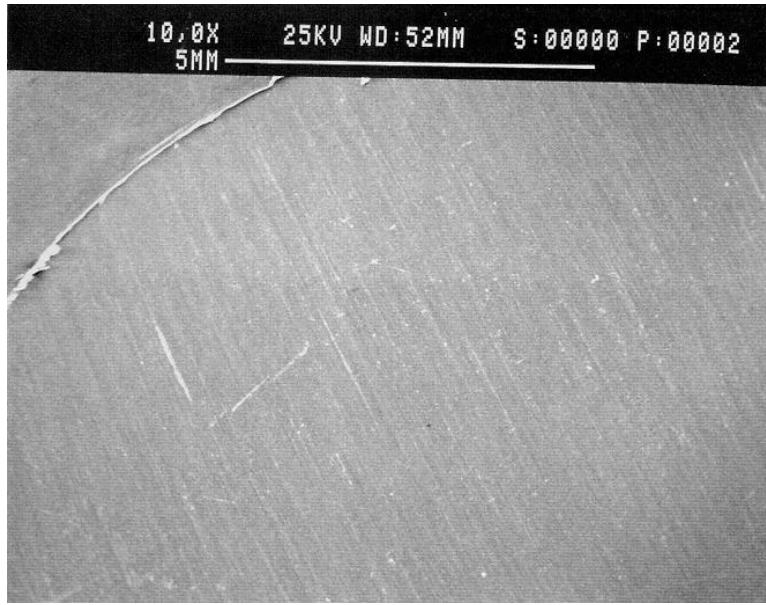


Figure 1-4. SPIFEX Witness Coupon 1, 10X

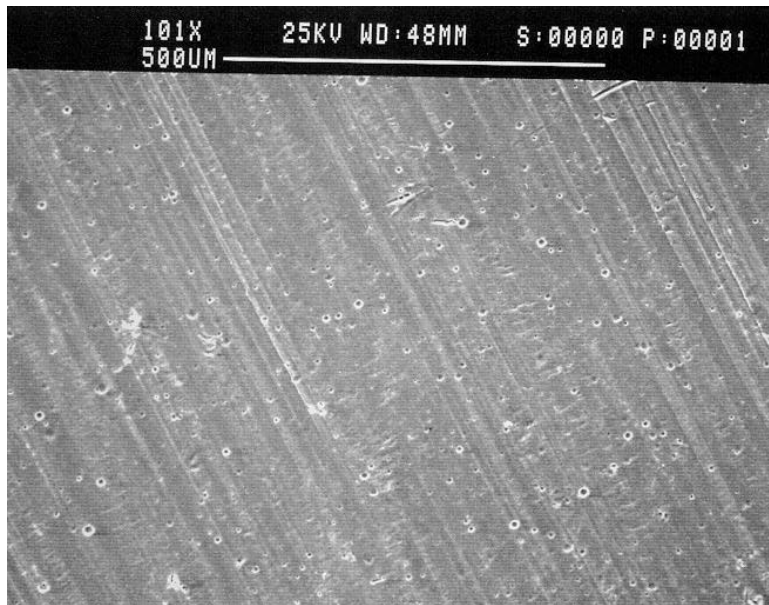


Figure 1-5. SPIFEX Witness Coupon 1, 101X

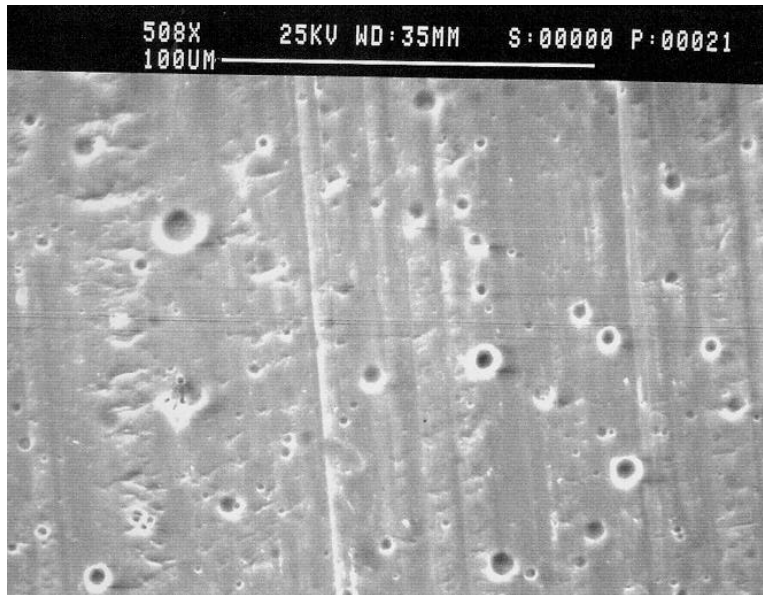


Figure 1-6 SPIFEX Witness Coupon 1, 508X

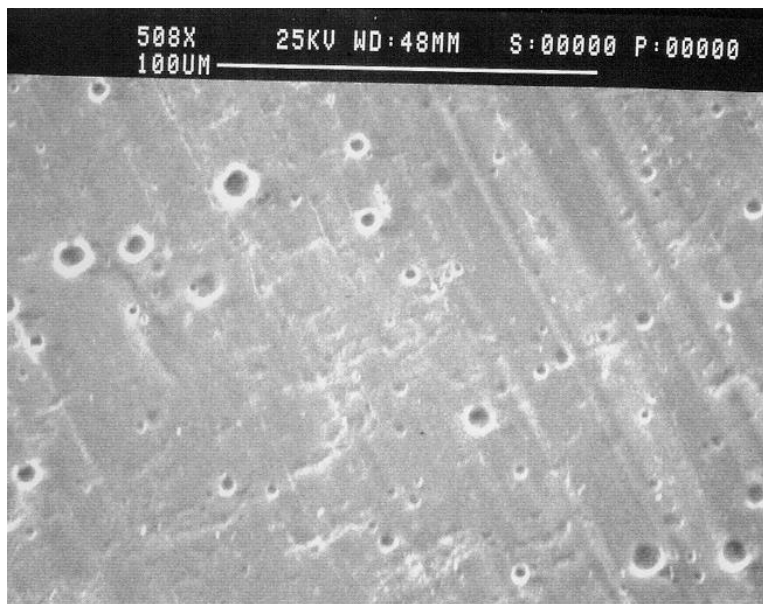


Figure 1-7. SPIFEX Witness Coupon 1, 508X

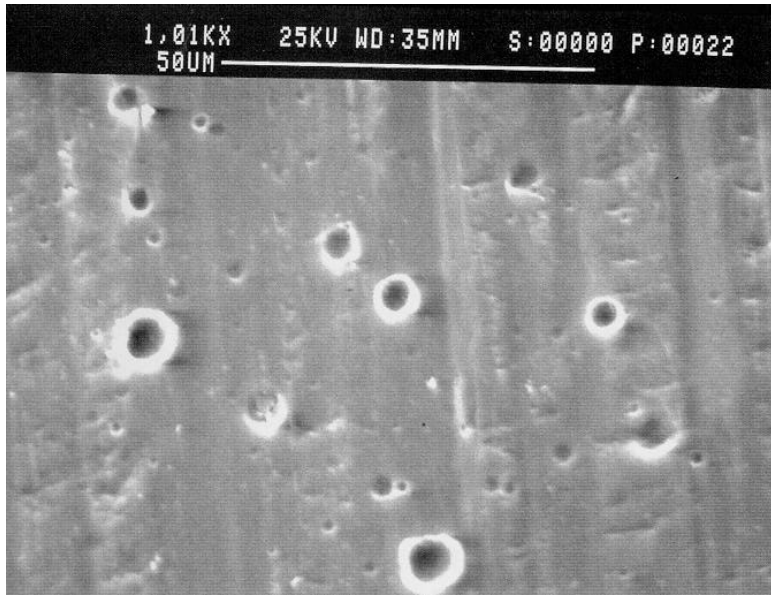


Figure 1-8. SPIFEX Witness Coupon 1, 1010X

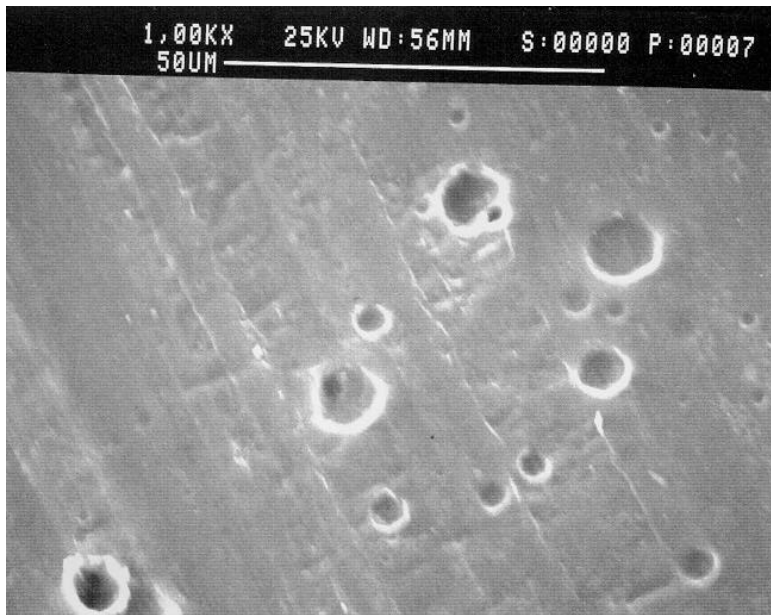


Figure 1-9. SPIFEX Witness Coupon 1, 1000X

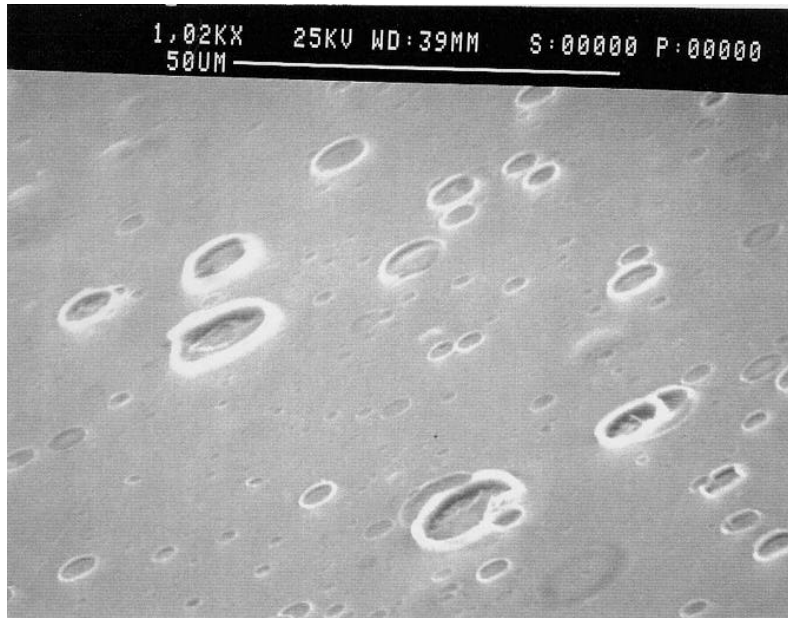


Figure 1-10. Kapton from Witness Coupon 1, 75a, 1020X



Figure 1-11. Kapton from Witness Coupon 1, 75a, 2070X

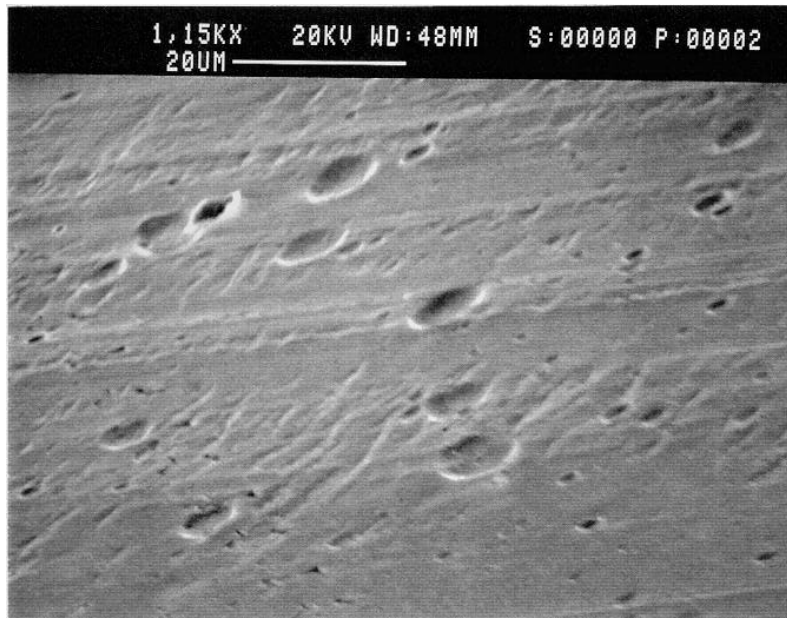


Figure 1-12. Witness Coupon 1, Aluminum Area 75a, 1150X



Figure 1-13. Witness Coupon 1, Aluminum Area 75a, 2070X

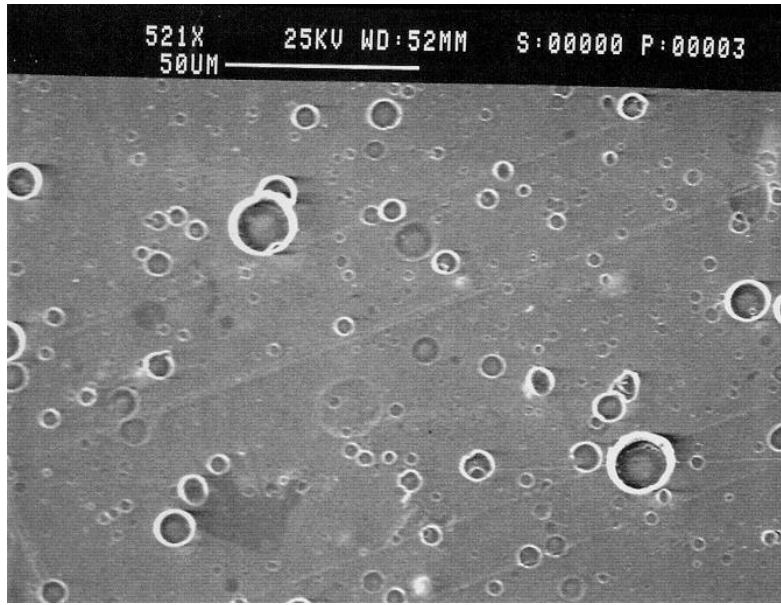


Figure 1-14. Kapton from Witness Coupon 1, 521X

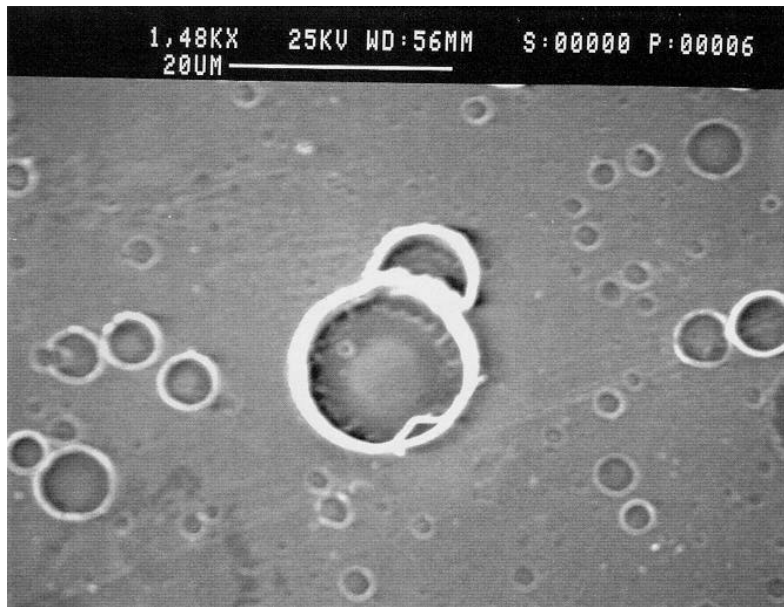


Figure 1-15. Kapton from Witness Coupon 1, 1480X



Figure 1-16. Witness Coupon 2, 10.5X

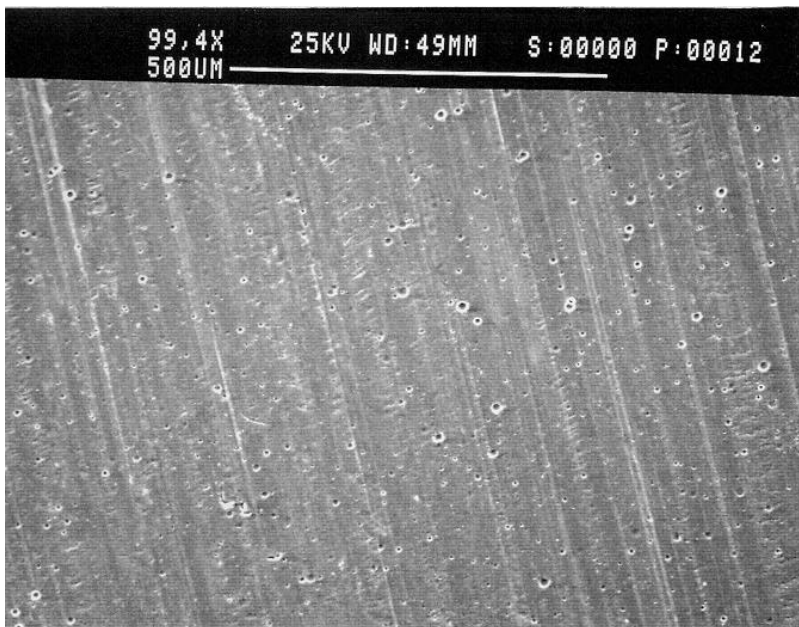


Figure 1-17. Witness Coupon 2, 99.4X

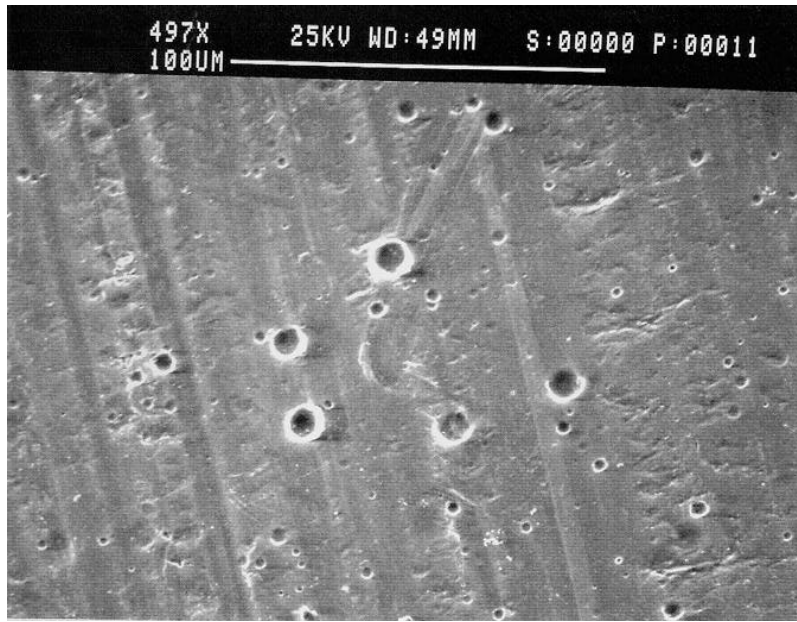


Figure 1-18. Witness Coupon 2, 497X

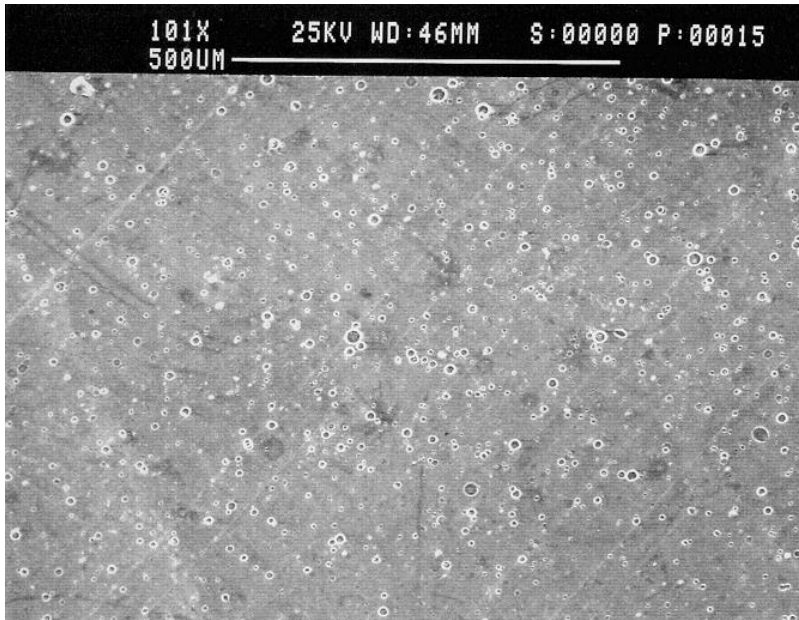


Figure 1-19. Kapton from Witness Coupon 2, 101X

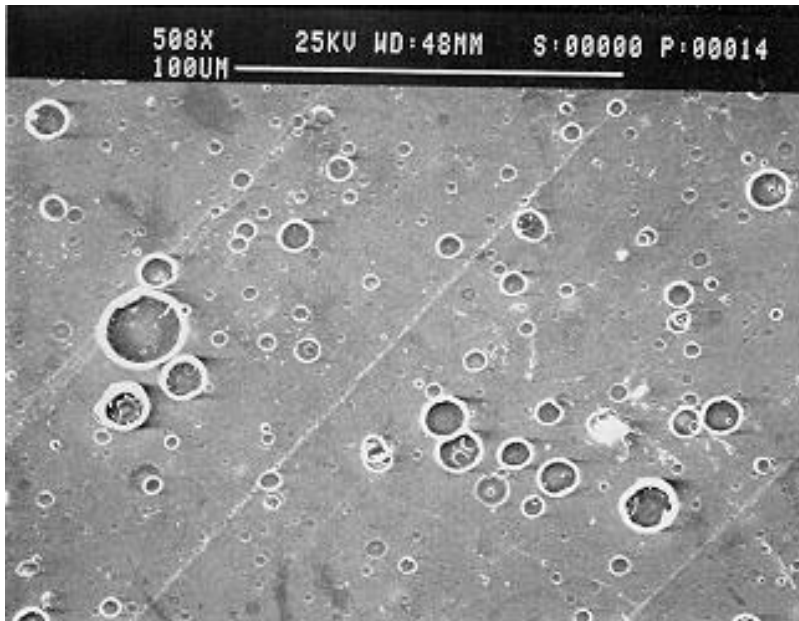


Figure 1-20. Kapton from Witness Coupon 2, 508X



Figure 1-21. Witness Coupon 3, 14.8X

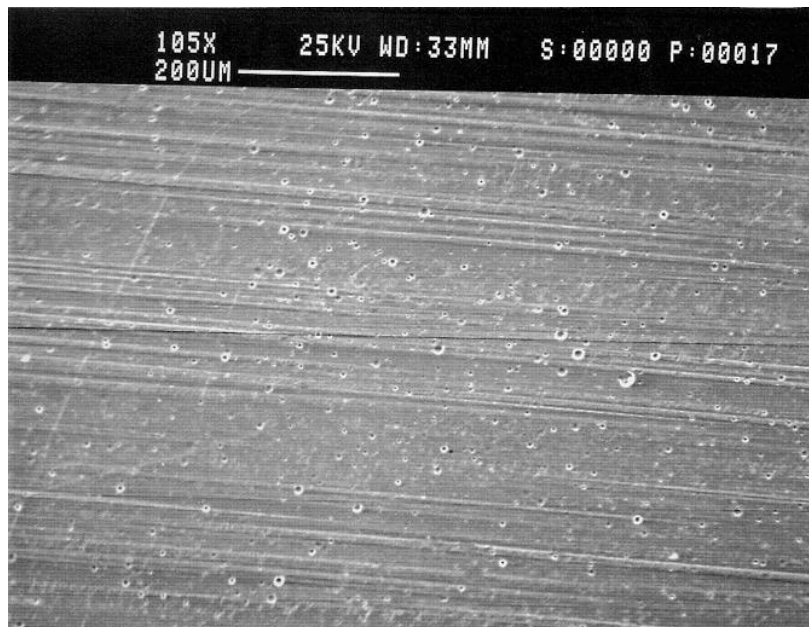


Figure 1-22. Witness Coupon 3, 105X

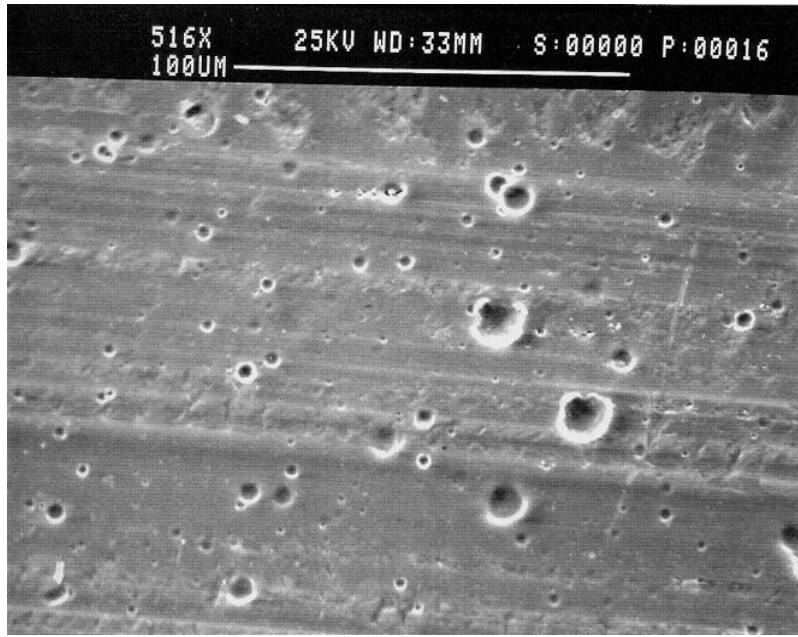


Figure 1-23. Witness Coupon 3, 516X



Figure 1-24. Kapton from Witness Coupon 3, 103X

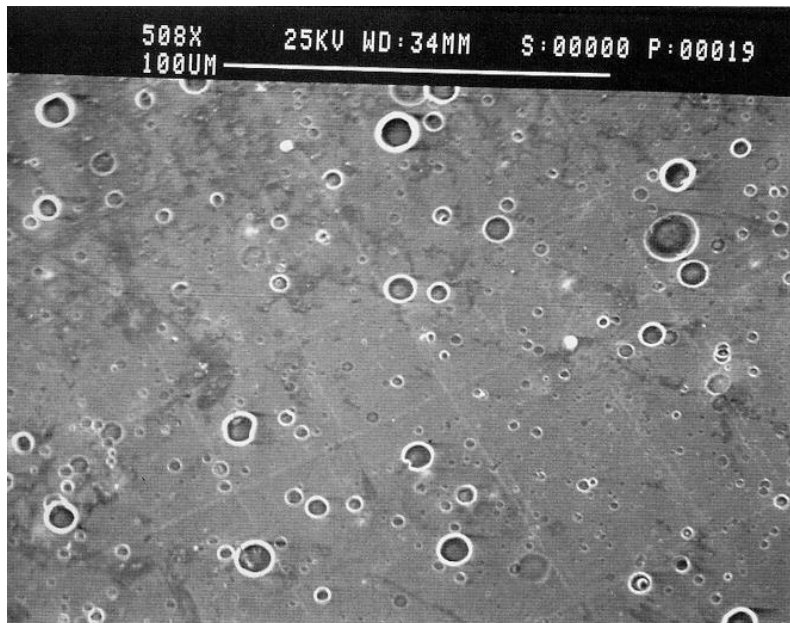


Figure 1-25. Kapton from Witness Coupon 3, 508X

The SPIFEX coupons and one identical ground control sample were examined using secondary electron imaging in a JEOL 35C SEM equipped with a Be-window EDS detector. This SEM is capable of determining all elements with atomic numbers higher than 10 and was operated at 20 kV during examinations.

No impact features were found in the ground control coupon. The first (and only) SPIFEX coupon examined had a high number density of small impact craters (Figure 2-1), although the surface was not saturated with craters. The craters generally measured less than 10 micrometers in diameter. Most impact features were typical round craters with raised rims (as shown in Figure 2-2); however, many elongate impact features were evident (Figure 2-3) indicating oblique impacts. Some of the smaller elongate features possibly represent secondary craters but this is speculation.

EDS analysis of approximately 100 impact crater interiors revealed that only about 5% contained any impactor residue material identifiable by this survey technique. Three craters contained solid material (interpreted as impactor residue) containing Fe in some form (Figure 2-4). Two craters contained Cr as a residue (Figure 2-3). That these residues contain Fe and Cr in the reduced state is speculation because an analysis for O was not performed to verify this.

The results of this study indicate that approximately 5% of the SPIFEX impact craters contain impactor residue, and those that do contain either Fe or Cr. The low percentage of craters containing surviving impactor residue is typical of these sorts of microcraters. For example, only about 2 to 4% of impact craters on the LDEF satellite were found by SEM to contain surviving impactor residue. Sometimes, thin vapor-deposited films from otherwise obliterated impactors can be detected by ion probe or various spectroscopic techniques, and these techniques may be applied if additional information is required.

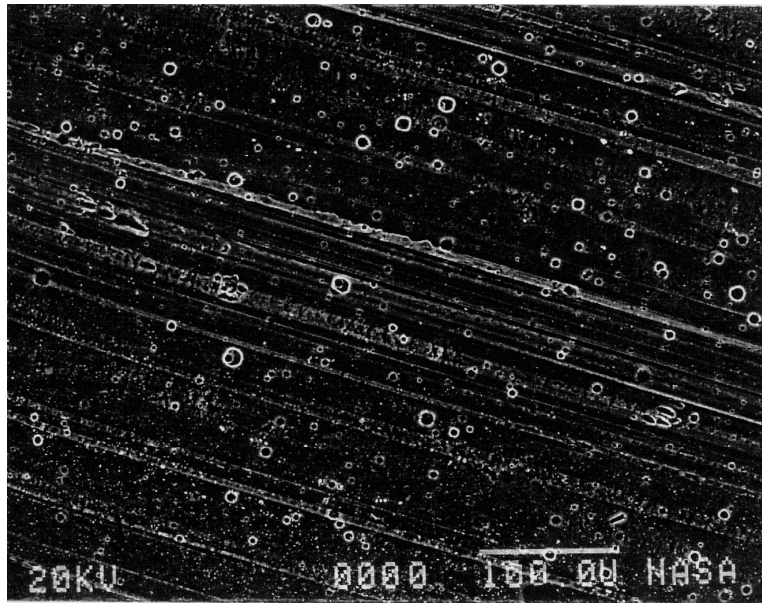


Figure 2-1. Typical view of SPIFEX flight coupon 1 showing many small craters.

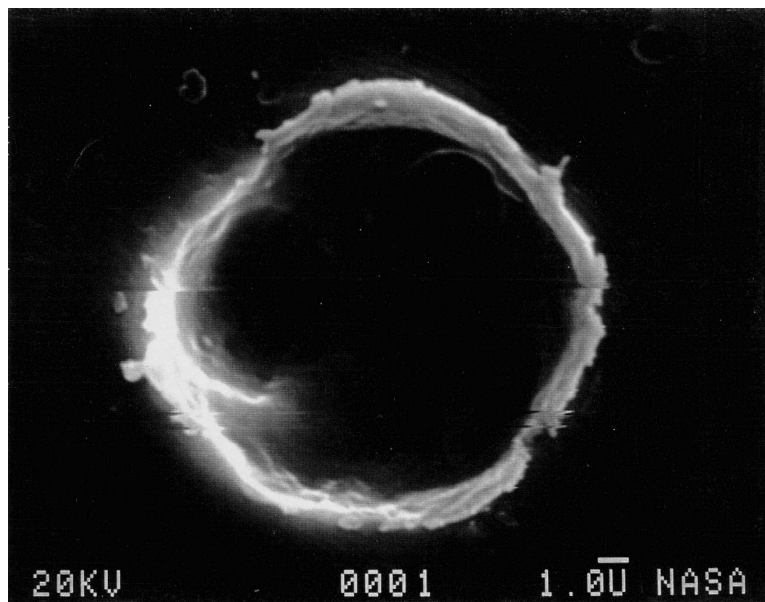


Figure 2-2. Typical round crater; this one contains no detectable impactor residue.

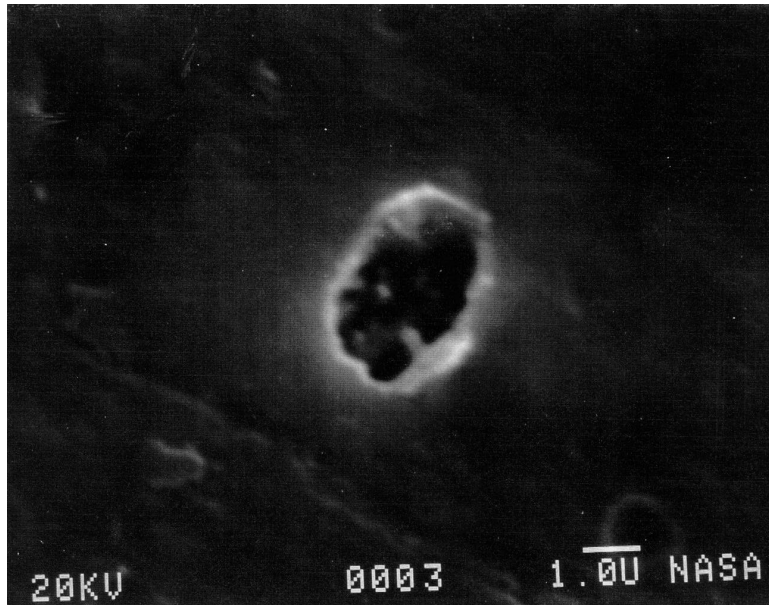


Figure 2-3. Elliptical crater with Cr-containing grains (all measuring less than 0.3 micrometers), interpreted as forming from an oblique impact by a Cr-containing impactor.

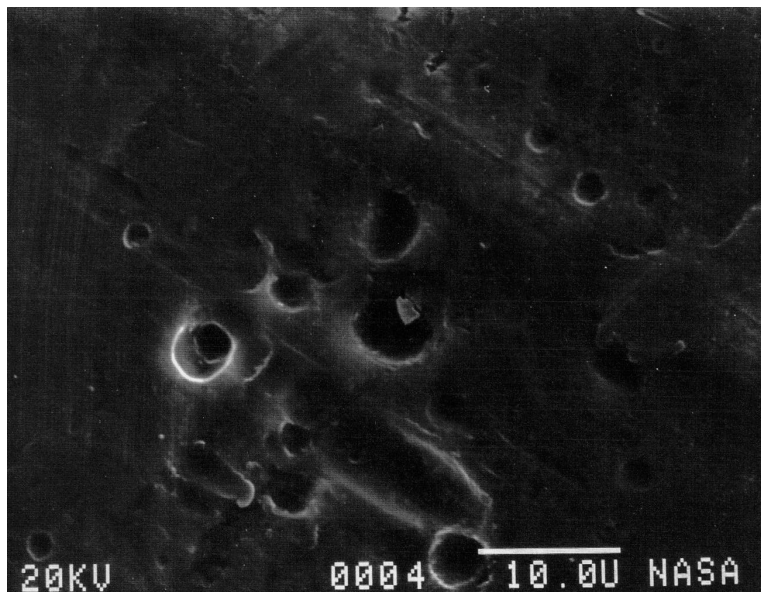


Figure 2-4. The crater in the center has a small grain (approximately 1 micrometer) of Fe, interpreted as being residue from an Fe-bearing impactor.